Sulfur Oxyacids and Radicals in the Gas Phase. A Variable-Time Neutralization−Photoexcitation−Reionization Mass Spectrometric and Ab Initio/RRKM Study

Aaron J. Frank, Martin Sadílek, Jordan G. Ferrier, and František Tureček*

Contribution from the Department of Chemistry, Bagley Hall, Box 351700, University of Washington, Seattle, Washington 98195-1700

Received July 30, 1997[⊗]

Abstract: Hydroxysulfinyl radical (**1**), hydrogensulfonyl radical (**2**), and dihydroxysulfane (**6**) were generated in the gas phase by collisional reduction of the corresponding cations and studied by the variable-time and photoexcitation methods of neutralization−reionization mass spectrometry and by ab initio and RRKM calculations. Radicals **1** and **2** were thermodynamically and kinetically stable. Two rotamers of **1**, *syn*-**1** and *anti*-**1**, were found computationally to be local energy minima. The computations suggested a complex potential energy surface for dissociations of **1**. The minimum-energy reaction path was the rate-determining isomerization to **2** followed by fast loss of H$^{\bullet}$ to form SO_2. Direct H$^{\bullet}$ loss from **1** was kinetically disfavored. Cleavage of the S−OH bond in **1** was highly endothermic and became kinetically significant at excitations >325 kJ mol^{-1}. In contrast to ab initio/RRKM predictions, **1** formed by vertical reduction of hydroxysulfinyl cation (**1**$^+$) dissociated mainly to OH$^{\bullet}$ and SO, whereas loss of H$^{\bullet}$ was less significant. Both dissociations showed microsecond kinetics as established by variable-time measurements. Photoexcitation of nondissociating **1** opened the H-loss channel, whereas collisional excitation did not change the branching ratio for the H$^{\bullet}$ and OH$^{\bullet}$ loss channels. The experimental results pointed to the formation of a large fraction of metastable and dissociative excited electronic states of **1** upon vertical electron transfer. Radical **2** was cogenerated with **1** by vertical reduction of a mixture of **1**$^+$ and **2**$^+$ produced by highly exothermic protonation of SO_2 with H_3^+. Pronounced loss of H$^{\bullet}$ from **2** occurred following collisional neutralization in accordance with RRKM predictions. Dihydroxysulfane (**6**) was stable following collisional neutralization of the cation-radical **6**$^{\bullet+}$. The G2(MP2) potential energy surface predicted the isomerization to hydrogensulfinic acid (**7**) followed by loss of water to be the lowest-energy dissociation of **6**. RRKM calculations showed the **6** → **7** isomerization to be the rate-determining step. Cation-radical **6**$^{\bullet+}$ also eliminated water through unimolecular isomerization to a stable nonclassical isomer, OS$^{\bullet+}$···H$_2$O (**9**). The thermochemistry of the neutral and ionic systems is discussed. The important role of excited electronic states in the formation of radicals by vertical electron transfer is emphasized.

Introduction

The tropospheric oxidation of hydrogen sulfide to sulfur dioxide is a multiple-step process that involves several transient intermediates.[1] The oxidation cascade is believed to start with the reaction of hydrogen sulfide with the hydroxyl radical to give HS$^{\bullet}$, which then undergoes further oxidations with O_2,[2−7] O_3,[4,8−10] NO,[3,11] or NO_2[2−6,12,13] to form oxygenated sulfur molecules. Intermediates relevant to the early stages of the oxidation process have been studied by high-level ab initio calculations, which provided relative energies and enthalpies of formation for HSO$^{\bullet}$ and SOH$^{\bullet}$.[14−16]

In addition to computational studies, several transient sulfur intermediates relevant to atmospheric processes were generated by collisional neutralization of the corresponding gas-phase cations and characterized by neutralization−reionization mass spectrometry (NRMS).[17−24] NRMS utilizes fast beams of stable mass-selected cations or anions, which are neutralized by glancing collisions with thermal atomic or molecular targets.[25] Due to the short interaction time between the fast ion and the target (<10^{-14} s), the electron transfer to the cation is considered

⊗ Abstract published in *Advance ACS Abstracts,* December 1, 1997.

(1) Tyndall, G. S.; Ravishankara, A. R. *Int. J. Chem. Kinet.* **1991**, *23*, 483−527.
(2) Tiee, J. J.; Wampler, F. B.; Oldenborg, R. C.; Rice, W. W. *Chem. Phys. Lett.* **1981**, *82*, 80−84.
(3) Black, G. *J. Chem. Phys.* **1984**, *80*, 1103−1107.
(4) Friedl, L. L.; Brune, W. H.; Anderson, J. G. *J. Phys. Chem.* **1985**, *89*, 5505−5510.
(5) Stachnik, R. A.; Molina, M. M. *J. Phys. Chem.* **1987**, *91*, 4603−4606.
(6) (a) Wang, N. S.; Lovejoy, E. R.; Howard, C. J. *J. Phys. Chem.* **1987**, *91*, 5743−5749. (b) Lovejoy, E. R.; Wang, N. S.; Howard, C. J. *J. Phys. Chem.* **1987**, *91*, 5749−5755.
(7) Schindler, R. N.; Benter, T. *Ber. Bunsenges. Phys. Chem.* **1988**, *92*, 558.
(8) Becker, K. H.; Inicencio, M. A.; Schurath, U. *Int. J. Chem. Kinet., Symp*. **1975**, *1*, 205−220.
(9) Schonle, G.; Rahman, M. M.; Schindler, R. N. *Ber. Bunsenges. Phys. Chem.* **1987**, *91*, 66−75.
(10) Wang, N. S.; Howard, C. J. *J. Phys. Chem.* **1990**, *94*, 8787−8794.
(11) Black, G.; Patrick, R.; Jusinski, L. E.; Slanger, T. G. *J. Chem. Phys.* **1984**, *80*, 4065−4070.
(12) Bulatov, V. P.; Kosliner, M. Z.; Sarkisov, O. M. *Khim. Fiz.* **1984**, *3*, 1300−1305; **1985**, *4*, 1353−1357.
(13) Lee, Y.-Y.; Lee, Y.-P.; Wang, N. S. *J. Chem. Phys.* **1994**, 387−392.
(14) Moore Plummer, P. L. *J. Chem. Phys.* **1990**, *92*, 6627−6634.
(15) Xantheas, S. S.; Dunning, T. H., Jr. *J. Phys. Chem.* **1993**, *97*, 6616−6627.
(16) Wilson, C.; Hirst, D. M. *J. Chem. Soc., Faraday Trans.* **1994**, *90*, 3051−3059.
(17) Iraqi, M.; Goldberg, N.; Schwarz, H. *J. Phys. Chem.* **1994**, *98*, 2015−2017.
(18) Egsgaard, H.; Carlsen, L.; Florencio, H.; Drewello, T.; Schwarz, H. *Chem. Phys. Lett.* **1988**, *148*, 537−540.
(19) Turecek, F.; Drinkwater, D. E.; McLafferty, F. W. *J. Am. Chem. Soc.* **1989**, *111*, 7696−7701.
(20) Gu, M.; Turecek, F. *J. Am. Chem. Soc.* **1992**, *114*, 7146−7151.
(21) Iraqi, M.; Goldberg, N.; Schwarz, H. *Int. J. Mass Spectrom. Ion Processes* **1993**, *124*, R7−9.
(22) Iraqi, M.; Schwarz, H. *Chem. Phys. Lett.* **1994**, *221*, 359−362.
(23) Frank, A. J.; Sadilek, M.; Ferrier, J. G.; Turecek, F. *J. Am. Chem. Soc.* **1996**, *118*, 11321−11322.
(24) Sadilek, M.; Turecek, F. *J. Phys. Chem.* **1996**, *100*, 15027−15032.

S0002-7863(97)02602-4 CCC: $14.00

Scheme 1

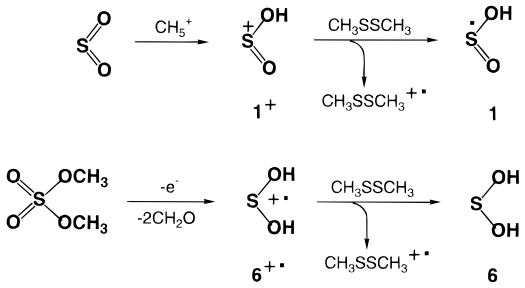

to be a nonresonant vertical process. This mandates that the fast neutral species be formed with the geometry of the precursor ion in the particular vibrational and rotational state. The internal energy of the neutral species depends mainly on the precursor ion energy and the Franck−Condon effects in vertical electron transfer.[26,27]

Relatively little is known about the oxygenated sulfur radicals and molecules corresponding to the general formula $[H_n,S,O_2]$, which may represent direct precursors of SO_2.[1] $[H,S,O_2]$ radicals were also considered as intermediates in SO_2-seeded flames,[28] and in the high-temperature reaction of SO_2 with H_2.[29] Recently, several ab initio studies addressed the relative stabilities of $[H,S,O_2]$ radicals and $[H_2,S,O_2]$ molecules and the thermochemistry of unimolecular dissociations and bimolecular reactions.[30−35] These calculations agreed that the hydroxysulfinyl radical, HO-SO•, **1**, was the most stable $[H,S,O_2]^•$ isomer and also provided relative energies for hydrogensulfonyl radical, H-SO_2•, **2**, peroxysulfhydryl radical, HS-O-O•, **3**, and hydroperoxysulfur radical, H-O-O-S• (**5**).[32] In addition, dihydroxysulfane (**6**), hydrogensulfinic acid (**7**), and a few other $[H_2,S,O_2]$ isomers have been characterized computationally as local energy minima.[34,35]

A preliminary communication from this laboratory reported on the first preparation of **1** and **6**, in the gas phase.[23] Radical **1** was generated by collisional neutralization of protonated sulfur dioxide, HO-SO^+ ($\mathbf{1}^+$), whereas **6** was prepared from its cation radical $\mathbf{6}^{•+}$ (Scheme 1). Species **1** and **6** were found to be stable and were characterized by NRMS in the form of reionized $\mathbf{1}^+$, $\mathbf{6}^{•+}$, and fragment ions. In the present report we examine the formation and dissociations of **1**, **2**, and **6** by combining computational methods with variable-time[36] and photodissociation measurements.[37] These studies converge on providing evidence that *a predominant fraction of unimolecular dissociations* of **1** formed by collisional electron transfer do not occur on the potential energy surface of the ground electronic state and therefore *must involve metastable excited states*.

Experimental Section

Methods. Measurements were made on a tandem quadrupole acceleration-deceleration mass spectrometer, as described previously.[38] Precursor cations were generated in a tight chemical ionization source at 200−220 °C. Protonations were performed with CH_5^+/CH_4 and H_3^+/H_2 chemical ionization; deuteronations were performed with CD_5^+/CD_4. The pressure of the protonation or deuteronation reagent gas was adjusted to 1.4×10^{-4} Torr in order to achieve $[M + H]^+/[M^{•+}]$ or $[M + D]^+/[M^{•+}]$ ratios >20 in most instances and keep the contributions from ^{33}S and ^{34}S isotopomers of sulfur dioxide cation-radicals below 0.1% of the $[M + H,D]^+$ ion intensities. Stable cations of 8200 eV kinetic energy and >25 μs lifetimes were neutralized by collisions with dimethyl disulfide, di-*n*-butylamine, or aniline, which were admitted to the collision cell at pressures such to achieve 70% transmittance of the ion beam. Neutral lifetimes were 3.8−3.9 μs for **1**−**6** in the conventional NR mass spectra. The neutral intermediates were reionized by collisions with O_2 at pressures such as to achieve 70% transmittance of the precursor ion beam. The NR conversions for $\mathbf{1}^+$ expressed as sums of integrated reionized peak intensities ($\sum I_{NR}$) relative to the intensity of the incident precursor ion beam (I_0) were $\sum I_{NR}/I_0 = (3.1 \pm 1.5) \times 10^{-5}$ from four measurements. By comparison, NR of $SO_2^{•+}$ gave $\sum I_{NR}/I_0 = 1.1 \times 10^{-5}$. Typically, 25−40 repetitive scans were accumulated per spectrum, and the spectra were reproduced in subsequent runs and over a period of several weeks.

Variable-time measurements were performed as described previously.[36] For laser photoexcitation experiments, the tandem mass spectrometer was equipped with an argon-ion laser, as described recently.[37] The neutralized beam passed through a 16.5 kV/cm electrostatic field gradient to remove high Rydberg states,[24,37] and it was merged with polarized light from a Laser Ionics 1400-12A Ar-ion laser operated in the power mode that delivered a total of 11 W at the 488 and 514.4 nm main visible lines (2.54 and 2.41 eV, respectively). The neutralization target was transparent at the wavelengths used.[37c] The photoexcitation experiments were conducted with two different potential settings on the drift region lenses. In one set of experiments, the electrostatic potentials on the conduit elements were maintained at +250 V, so that any ions formed within the conduit had incorrect combinations of kinetic and potential energies and were rejected.[38] The neutral species and their photodissociation products were collisionally reionized in the downbeam cell after 3.8 μs. In another set of experiments, oxygen was introduced in the conduit, and the electrostatic potentials were scanned in link with the deceleration lens potentials to allow detection of survivor and product ions formed within the conduit between the deflector lens and the reionization cell.[38] This provided a 0.3−2.8 μs observation window for the neutral intermediates to be photoexcited and collisionally reionized. This also increased the observation window for ion dissociations by 3.5 μs. Over 50 repetitive scans were accumulated per spectrum with the laser on and off in order to correct for background effects. Difference spectra were obtained by subtracting the integrated peak intensities measured with the laser on and laser off. To account for the ±20% variations in the total NR ion currents, the laser-on spectra were normalized to the value from the laser-off measurement and averaged over several multiscan spectra.

Collisionally activated dissociation (CAD) spectra were measured on a Kratos Profile HV-4 double-focusing sector mass spectrometer as described previously.[20] Oxygen was used as the collision gas at 70% transmittance of the precursor ion beam.

Materials. Methane (Matheson, 99.97%), hydrogen (Air Liquid, 99.99%), CD_4 (Cambridge Isotope Laboratories, 99% D), dimethyl

(25) (a) Danis, P. O.; Wesdemiotis, C.; McLafferty, F. W. *J. Am. Chem. Soc.* **1983**, *105*, 7454−7456. For recent reviews, see: (b) Goldberg, N.; Schwarz, H. *Acc. Chem. Res.* **1994**, *27*, 347−352. (c) Turecek, F. *Org. Mass Spectrom.* **1992**, *27*, 1087. (d) McLafferty, F. W. *Int. J. Mass Spectrom. Ion Processes* **1992**, *118/119*, 221.
(26) Holmes, J. L. *Mass Spectrom. Rev.* **1989**, *8*, 513−539.
(27) Nguyen, V. Q.; Turecek, F. *J. Mass Spectrom.* **1996**, *31*, 843−854.
(28) (a) McDowell, C. A.; Herring, F. G.; Tait, J. C. *J. Chem. Phys.* **1975**, *65*, 3278−3283. (b) Kallend, A. S. *Combust. Flame* **1972**, *19*, 227. (c) Cullis, C. F.; Mulcahy, M. F. R. *Combust. Flame* **1972**, *18*, 225. (d) Zachariah, M. R.; Smith, O. I. *Combust. Flame* **1987**, *69*, 125−139.
(29) Arutyunov, V. A.; Vedeneev, V. I.; Ushakov, V. A.; Shumova, V. V. *Kinet. Catal.* **1990**, *31*, 6−11.
(30) Binns, D.; Marshall, P. *J. Chem. Phys.* **1991**, *95*, 4940−4947.
(31) Morris, V.; Jackson, W. M. *Chem. Phys. Lett.* **1994**, *223*, 445−451.
(32) Laakso, D.; Smith, C. E.; Goumri, A.; Rocha, J.-D. R.; Marshall, P. *Chem. Phys. Lett.* **1994**, *227*, 377−383.
(33) Qi, J.-X.; Deng, W.-Q.; Han, K.-L.; He, G.-Z. *J. Chem. Soc., Faraday Trans.* **1997**, *93*, 25−28.
(34) Moore Plummer, P. L.; Chen, T. S.; Law, K. Y. *Atmos. Environm.* **1984**, *18*, 2769−2774.
(35) Laakso, D.; Marshall, P. *J. Phys. Chem.* **1992**, *96*, 2471−2474.
(36) (a) Kuhns, D. W.; Tran, T. B.; Shaffer, S. A.; Turecek, F. *J. Phys. Chem.* **1994**, *98*, 4845−4853. (b) Kuhns, D. W.; Turecek, F. *Org. Mass Spectrom.* **1994**, *29*, 463−469. (c) Sadilek, M.; Turecek, F. *J. Phys. Chem.* **1996**, *100*, 224−232.
(37) (a) Sadilek, M.; Turecek, F. *J. Phys. Chem.* **1996**, *100*, 9610−9614. (b) Sadilek, M.; Turecek, F. *Chem. Phys. Lett.* **1996**, *263*, 203−208. (c) Nguyen, V. Q.; Sadilek, M.; Frank, A. J.; Ferrier, J. G.; Turecek, F. *J. Phys. Chem. A* **1997**, *101*, 3789−3799.
(38) Turecek, F.; Gu, M.; Shaffer, S. A. *J. Am. Soc. Mass Spectrom.* **1992**, *3*, 493−501.

disulfide, di-*n*-butylamine, aniline, dimethyl sulfate, and di(methyl-d_3)sulfate (99% D, all Aldrich) were used as received. The neutralization reagents were carefully degassed by several freeze−pump−thaw cycles before use.

Calculations. Standard ab initio calculations were performed using the Gaussian 94 suite of programs.[39] Geometries were optimized with HF/6-31+G(d,p) calculations and further reoptimized with MP2(FULL)/6-31+G(d,p).[40] Harmonic vibrational frequencies were calculated to characterize local minima and saddle points. The HF/6-31+G(d,p) frequencies were scaled by 0.893, and the MP2(FULL)/6-31+G(d,p) frequencies were scaled by 0.93[41] and used to calculate zero-point vibrational energies (ZPVE), 298 K enthalpy corrections, and heat capacities using the rigid-rotor-harmonic oscillator approximation. Single point energies were obtained with the Gaussian 2(MP2) scheme.[42] The calculated total energies, frequencies, and ZPVE are available as Supporting Information. For open-shell systems, the UMP2 calculations gave $\langle S^2 \rangle$ values of 0.76−0.77 for most doublets and 2.02−2.05 for triplets indicating only minor spin contamination, which was further reduced by Schlegel's annihilation procedure.[43] RRKM calculations were performed using Hase's program.[44] Vibrational state densities were obtained by direct count for internal energies up to 20 kJ mol^{-1} above the dissociation threshold, while the Whitten-Rabinovitch approximation was used at higher energies.[45] The rotational states were treated adiabatically in the RRKM calculations.[46] The microscopic rate constants, *k(E,J,K)*, were Boltzmann-averaged over the thermal distribution of rotational *J* and *K* states pertinent to the ion source temperature.[37c]

Results

Ion and Neutral Energetics in the [H,S,O$_2$] System. The calculated relative energies are presented first and compared with the previously reported data from ab initio calculations. The calculated energetics and RRKM kinetics are then used to aid in the interpretation of experimental data.

Addition of a proton to sulfur dioxide can give rise to various $[H,S,O_2]^+$ ion isomers; only singlet ions were relevant to the present experiments, and therefore triplet states were not considered. The optimized structures are shown in Figure 1; the relative enthalpies are given in Table 1. The hydroxysulfinyl ion $\mathbf{1}^+$ corresponding to O-protonation in sulfur dioxide exists as two planar rotamers, *syn*-$\mathbf{1}^+$ and *anti*-$\mathbf{1}^+$ (Figure 1). The higher stability of *syn*-$\mathbf{1}^+$ ion can be ascribed to the more favorable dipolar interactions between the H−O and O−S bond dipoles than in *anti*-$\mathbf{1}^+$. The hydrogensulfonyl ion $\mathbf{2}^+$, corresponding to S-protonation in sulfur dioxide, the O-protonated sulfur peroxide ion $\mathbf{3}^+$, and the cyclic isomer $\mathbf{4}^+$ were calculated as potential energy minima 176, 405, and 415 kJ mol^{-1} less stable, respectively, than *syn*-$\mathbf{1}^+$ (Table 1). Attempts at obtaining an optimized structure for the singlet H−S−O−O$^+$ isomer ($\mathbf{5}^+$) failed because of severe SCF convergence problems. It cannot be excluded, however, that $\mathbf{5}^+$ exists as a high-energy triplet state by analogy with the triplet CH_3O^+ ion.[47]

Table 1. Relative Enthalpies of $[H,S,O_2]^+$ Ions[a]

ion/reaction	ΔH_0	ΔH_{298}
syn-$\mathbf{1}^+$	0	0
syn-$\mathbf{1}^+$(VI)[b]	28	
anti-$\mathbf{1}^+$	8.7	8.8
$\mathbf{2}^+$	176	176
$\mathbf{3}^+$	405	405
$\mathbf{4}^+$	415	415
$SO^{\bullet+} + OH^{\bullet}$	430	438
$SO_2^{\bullet+} + H^{\bullet}$	508	514
$(^3A'')SOH^+ + (^3P)O$	549	554

[a] From spin-projected G2(MP2) energies in kJ mol^{-1}. [b] Vertical ionization of *syn*-**1**.

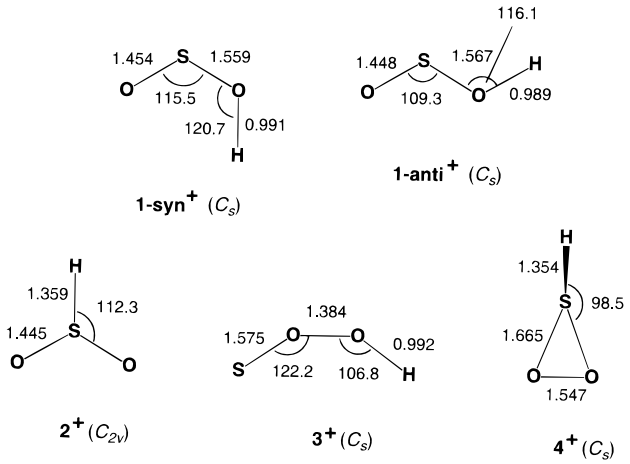

Figure 1. MP2(FULL)/6-31+G(d,p) optimized geometries of $[H,S,O_2]^+$ cations. Bond lengths in Å, bond and dihedral angles in deg.

Ab initio calculations of sulfur species with split-valence basis sets can give inaccurate equilibrium geometries and relative energies for some systems.[48,49] The $[H,S,O_2]^+$ ion system allowed us to compare the calculated relative energies with reliable experimental proton affinities (PA), heats of reaction ($\Delta H^o_{r,298}$), and ionization energies (IE) and thus to estimate the errors inherent to our computational approach. The calculated PA of SO_2 (640 kJ mol^{-1}) was slightly overestimated against the experimental values of 636 and 631 kJ mol^{-1}.[50,51] However, this small difference was diminished upon accounting for the formation of an equilibrium mixture of *syn*-**1** (85%) and *anti*-$\mathbf{1}^+$ (15%) at the experimental temperature of 600 K.[51] The Boltzmann-weighed proton affinity, 638 kJ mol^{-1}, showed an improved agreement with the experimental values.

The 298 K dissociations of $\mathbf{1}^+$ to ($SO_2^{\bullet+} + H^{\bullet}$) and ($SO^{\bullet+} + OH^{\bullet}$) were 514 and 438 kJ mol^{-1} endothermic, respectively, from experimental $\Delta H^o_{r,298}$ data.[50b] These exothermicities were matched by the calculated $\Delta H_{r,298}$ (Table 1). Good agreement

(39) *Gaussian 94 (Revision D.1)*: Frisch, M. J.; Trucks, G. W.; Schlegel, H. B.; Gill, P. M. W.; Johnson, B. G.; Robb, M. A.; Cheeseman, J. R.; Keith, T. A.; Petersson, G. A.; Montgomery, J. A.; Raghavachari, K.; Al-Laham, M. A.; Zakrzewski, V. G.; Ortiz, J. V.; Foresman, J. B.; Cioslowski, J.; Stefanov, B. B.; Nanayakkara, A.; Challacombe, M.; Peng, C. Y.; Ayala, P. Y.; Chen, W.; Wong, M. W.; Andres, J. L.; Replogle, E. S.; Gomperts, R.; Martin, R. L.; Fox, D. J.; Binkley, J. S.; Defrees, D. J.; Baker, J.; Stewart, J. P.; Head-Gordon, M.; Gonzalez, C.; Pople, J. A. Gaussian, Inc.: Pittsburgh, PA, 1995.

(40) Turecek, F.; Cramer, C. J. *J. Am. Chem. Soc.* **1995**, *117*, 12243−12253.

(41) Hehre, W. J.; Radom, L.; Schleyer, P. v. R.; Pople, J. A. *Ab Initio Molecular Orbital Theory*; Wiley: New York, 1986.

(42) Curtiss, L. A.; Raghavachari, K.; Pople, J. A. *J. Chem. Phys.* **1993**, *98*, 1293−1298.

(43) Schlegel, H. B. *J. Chem. Phys.* **1986**, *84*, 4530−4534.

(44) Zhu, L.; Hase, W. L. *Quantum Chemistry Program Exchange*; Indiana University: Bloomington, IN, 1994; Program No. QCPE 644.

(45) Whitten, G. Z.; Rabinovitch, B. S. *J. Chem. Phys.* **1963**, *38*, 2466−2473.

(46) Zhu, L.; Hase, W. L. *Chem. Phys. Lett.* **1990**, *175*, 117−123.

(47) (a) Bouma, W. J.; Nobes, R. H.; Radom, L. *Org. Mass Spectrom.* **1982**, *17*, 315−317. (b) Uggerud, E.; Helgaker, T. *J. Am. Chem. Soc.* **1992**, *114*, 4265−4628.

(48) Smart, B. A.; Schiesser, C. H. *J. Comput. Chem.* **1995**, *16*, 1055−1066.

(49) Ruttink, P. J. A.; Burgers, P. C.; Francis, J. T.; Terlouw, J. K. *J. Phys. Chem.* **1996**, *100*, 9694−9697.

(50) (a) Lias, S. G.; Liebman, J. F.; Levin, R. D. *J. Phys. Chem. Ref. Data* **1984**, *13*, 695−808. (b) Lias, S. G.; Liebman, J. F.; Levin, R. D.; Kafafi, S. A. *NIST Standard Reference Database 19A*. National Institute of Standards and Technology, Gaithersburg, MD (1993). (c) Levin, R. D.; Lias, S. G. *Ionization Potential and Appearance Potential Measurements*, 1971−1981; National Bureau of Standards; NSRDS-NBS 71, U.S. Government Printing Office: Washington, D.C. 1982.

(51) (a) Szulejko, J. E.; McMahon, T. B. *J. Am. Chem. Soc.* **1993**, *115*, 7839−7848. (b) Szulejko, J. E., Revised Proton Affinity Data, University of Waterloo, April 1996.

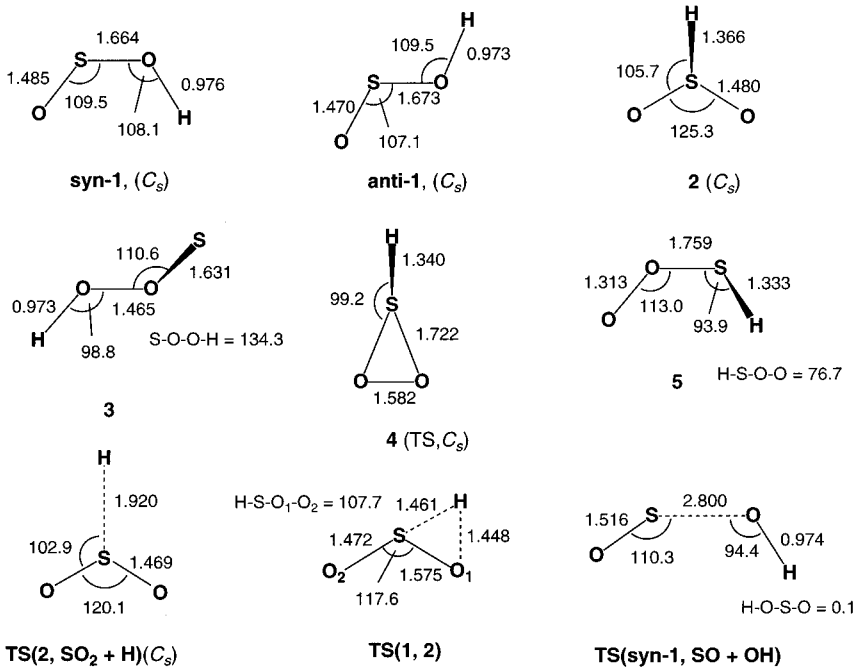

Figure 2. UMP2(FULL)/6-31+G(d,p) optimized geometries of $[H,S,O_2]^\bullet$ radicals.

Table 2. Relative Enthalpies of $[H,S,O_2]^\bullet$ Radicals[a]

radical/reaction	ΔH_0	ΔH_{298}
syn-**1**	0	0
syn-**1**(VN)[b]	27	
anti-**1**	7.5	7.6
2	102	104
3	307	307
4(TS)	447	446
5	358	358
$SO_2 + H^\bullet$	165	169
$(^3\Sigma^-)SO + OH^\bullet$	289	295
$(^1\Delta)SO + OH^\bullet$	376	376
syn-**1** $\rightarrow SOH^\bullet + (^3P)O$	484	486
TS(**1** $\rightarrow$ **1′**)	128	126
TS(**1** $\rightarrow$ **2**)	212	211
TS(**2** $\rightarrow SO_2 + H^\bullet$)	170	168

[a] From G2(MP2) energies in kJ mol^{-1}. [b] Vertical neutralization of *syn*-**1**$^+$.

was also obtained for the calculated IE_a of SO_2 and $(^3\Sigma^-)SO$ (12.31 and 10.22 eV, respectively), compared with the experimental values of 12.35 and 10.29 eV, respectively.[50b] This indicated that single-point G2(MP2) calculations based on MP2-(FULL)/6-31+G(d,p) optimized geometries can provide reasonably good estimates for the oxygenated sulfur species studied. Inclusion of the MP2/6-311+G(3df,2p) calculation in the G2-(MP2) scheme was critical for obtaining reliable relative energies.

Among $[H,S,O_2]$ radicals, *syn*-**1** (C_s, $^2A''$) was the most stable isomer in the ground electronic state (Figure 2, Table 2) in agreement with previous computational studies.[30−33] However, a planar anti-rotamer, *anti*-**1** (C_s, $^2A''$) was also obtained as a local energy minimum, which was 7.5 kJ mol^{-1} less stable than the syn isomer. The rotational barrier for the *syn*-**1** $\rightarrow$ *anti*-**1** interconversion was estimated at $E_{rot} = 20$ kJ mol^{-1} from eq 1,[52] where I_{red} is the reduced moment of inertia about the S−OH bond, ν is the torsional frequency (a''_1, 183 cm^{-1}), and r is the

$$E_{rot} = I_{red} \times 8\pi^2\nu^2/r^2 \qquad (1)$$

(52) Aston, J. G.; Fritz, J. J. *Thermodynamics and Statistical Thermodynamics*; Wiley: New York, 1959.

rotational degeneracy. Hence, *syn*-**1** and *anti*-**1** must interconvert rapidly at room temperature to reach thermal equilibrium preferring *syn*-**1**. The calculated ΔG^o_{298}(syn $\rightarrow$ anti) = 7.1 kJ mol^{-1} indicated 95% of *syn*-**1** at room temperature equilibrium.

The calculated IE_v of *syn*-**1** (9.06 eV) was slightly higher than the adiabatic value, $IE_a = 8.77$ eV. The vertical recombination energy (RE_v) of *syn*-**1**$^+$ was 8.49 eV. Thus, the Franck−Condon energies for the vertical formations of *syn*-**1** and *syn*-**1**$^+$ were 27−28 kJ mol^{-1}. The vibrational excitation in vertically formed *syn*-**1** was converted to an effective temperature (540 K) and used to calculate the rotamer distribution. The corresponding ΔG^o_{540}(syn $\rightarrow$ anti) = 6.3 kJ mol^{-1} gave a 80/20 mixture of *syn*-**1** and *anti*-**1** for the vertically formed radicals after vibrational energy redistribution and isomer equilibration. The calculated IE_a values for *anti*-**1** and **2**, 8.78 and 8.72 eV, respectively, were very similar to that for *syn*-**1**.

Relevant to our experimental studies (vide infra), the low excited electronic states in **1** were also of interest. Single-determinant calculations allow only the lowest state of a given symmetry to be obtained. The lowest $^2A'$ excited state of *syn*-**1** was constructed by promoting the electron from the 4a″ SOMO to the 14a′ LUMO. A single-point UMP2/6-31+G(d,p) calculation gave the $^2A'$ state energy which was 4.3 eV above that of the $(X)^2A''$ state. This implied that ground-state **1** could not be excited to the lowest $^2A'$ state by photons from the Ar-ion laser (488 and 514.5 nm) used in the photoexcitation experiments as discussed below. The other $[H,S,O_2]^\bullet$ isomers were substantially less stable than **1** (Figure 2, Table 2).[31−33] Radicals **2**, **3**, and **5** were found to be 102, 307, and 358 kJ mol^{-1} less stable, respectively, than *syn*-**1**. The cyclic structure **4** was a high-energy saddle point for degenerate isomerization in **5** (Table 2). Isomerization of *syn*-**1** to **2** required an activation barrier of 212 kJ mol^{-1}. Dissociation of **2** to SO_2 and $H^\bullet$ was calculated to be 63 kJ mol^{-1} endothermic and had to surmount an additional small barrier for the reverse hydrogen addition (5 kJ mol^{-1}, Table 2).[53] This indicated that addition of $H^\bullet$ to SO_2 to form **2** was dynamically barrierless at room temperature, since the combined thermal energies of the reactants were practically equal to the 298 K energy of the transition state.

The dissociation by direct cleavage of the O−H bond in *syn*-**1** and *anti*-**1** was also investigated computationally. Under C_s symmetry constraints, stretching the O−H bond in *anti*-**1** resulted in a steep increase of potential energy, e.g., 440 kJ mol^{-1} above *anti*-**1** at r(O−H) = 2.0 Å. However, this reaction path was found to follow a ridge, and upon releasing the C_s constraint, the system relaxed to follow the *anti*-**1** → **2** isomerization path. An attempted O−H bond dissociation in *syn*-**1** resulted in a degenerate isomerization by hydrogen migration between the oxygen atoms of 128 kJ mol^{-1} activation energy (Table 2). Hence, a direct loss of H$^\bullet$ from *syn*-**1** or *anti*-**1**, for which a substantial energy barrier was found by previous calculations,[31,33] was dynamically hampered. Dissociation of the S−OH bond in *syn*-**1** and *anti*-**1** was continuously endothermic requiring 289 kJ mol^{-1} at the thermochemical threshold at 0 K.

The present augmented G2(MP2) calculations agreed very well with the previous G2 calculations of Laakso et al.[32] and reasonably well with the MP2/6-311G(d,p) calculations of Qi et al.[33] and the MP4(SDTQ)/DZP calculations of Morris and Jackson.[31] Compared with Qi's data,[33] the augmented G2(MP2) gave a transition state for the isomerization to **2** which was 34 kJ mol^{-1} lower and a transition state energy for the degenerate rearrangement in *syn*-**1** which was 28 kJ mol^{-1} higher. The lower energy for TS(**1** → **2**) was primarily due to the MP2/6-311+G(3df,2p) calculation in the G2(MP2) scheme. The MP2-(FULL)/6-31+G(d,p) optimization found *anti*-**1** as a local minimum, contrary to Qi's conclusions but in agreement with the results of Morris and Jackson.[31] The latter authors obtained a large barrier for the dissociation of the H−S bond in **2**, which was 46 kJ mol^{-1} above the thermochemical threshold, and which may be due to the smaller basis set used in their single-point energy calculations. Morris and Jackson reported a 205 kJ mol^{-1} energy barrier for the addition of H$^\bullet$ to the oxygen terminus in SO_2, which was the reverse of the H−O bond dissociation in **1**.[31] However, they were unable to locate the transition state, which may be consistent with the symmetry forbidden character of the reaction on the potential energy surface of the ground electronic state. Qi et al. did find a large barrier for the O−H bond dissociation, which in their calculations required 284 kJ mol^{-1} above *syn*-**1**.[33]

RRKM Kinetics in the [H,S,O$_2$]$^\bullet$ System. The G2(MP2) potential energy surface for the ground electronic state was used to calculate microcanonical rate constants, *k(E)*, for the consecutive and competitive dissociations of **1** and **2** (Figure 3). The rate constant for the internal rotation in **1** was deemed to be at the rotational frequency limit (4.5×10^{13} s^{-1}) at all relevant excitation energies. The degenerate isomerization in *syn*-**1** was kinetically irrelevant for dissociations. Isomerization to **2** was the lowest-energy unimolecular reaction of **1**. However, the *k(E)* curves for the latter isomerization and dissociation to ($^3\Sigma^-$)SO and OH$^\bullet$ crossed at E = 325 kJ mol^{-1}. This implied that isomerization to **2** should predominate at vibrational excitations below the crossing point, whereas the S−OH bond cleavage should surpass the isomerization at excitations above the crossing point. Very similar *k*(E) curves were calculated for dissociations of **1D** and **2D**, which indicated small isotope effects on the branching ratios for loss of D and OD.

Radical **2**, when formed with an internal energy corresponding to the **1** → **2** isomerization threshold, was calculated to dissociate rapidly (log k = 12.8) to SO_2 and H$^\bullet$. Hence, the **1** → **2** isomerization was the rate-determining step in the overall dissociation. The reverse isomerization, **2** → **1**, was calculated to be 2−3 orders of magnitude slower than the dissociation to SO_2 and H$^\bullet$ (Figure 3). This may be somewhat mitigated by tunneling through the isomerization barrier, which would increase the rate constants for the **1** ⇄ **2** isomerization.

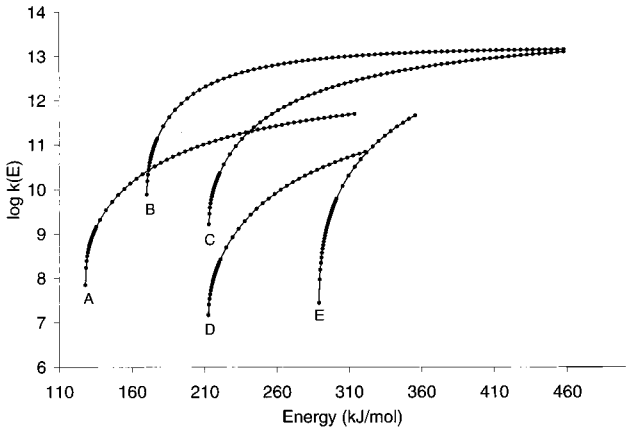

Figure 3. RRKM rate constants for unimolecular isomerizations and dissociations of **1** and **2**. The energy scale is common for all reactants and is referenced to **1** at 0 K. (A) *syn*-**1** → *syn*-**1′**; (B) **2** → SO_2 + H$^\bullet$; (C) **2** → **1**; (D) *anti*-**1** → **2**; (E) *syn*-**1** → ($^3\Sigma^-$) SO + OH$^\bullet$.

The combined energy and kinetic data allowed us to draw conclusions as to the formation of **1** by bimolecular reactions in the gas phase. The large energy barrier to H$^\bullet$ addition to the oxygen atoms in sulfur dioxide and the absence of a barrier to the addition to the sulfur atom to form **2** made structure **1** kinetically inaccessible through the direct addition channel. Moreover, the presence of the energy barrier for the isomerization of **2** to **1** inhibited the indirect pathway to **1**, except for leakage through tunneling effects. It follows that **1** cannot be formed classically by H$^\bullet$ atom addition to sulfur dioxide.

In contrast, the exothermic reaction of sulfur monoxide with OH$^\bullet$ was barrierless and may result in the formation of stable **1** if the environment provides efficient cooling through third-body collisions. At the thermochemical threshold of the OH$^\bullet$ addition (289 kJ mol^{-1} above *syn*-**1**), the unimolecular rate constant for the isomerization to **2** was calculated at 6×10^{11} s^{-1}. This substantially exceeded the typical collision rate at 25 °C and 1 atm, $k_{coll} \approx 4 \times 10^9$ s^{-1}. Hence, hot **1** formed by OH$^\bullet$ addition to SO was predicted to rapidly isomerize to **2** and dissociate to SO_2 and H$^\bullet$.

Formation and Dissociations of SO$_2$H$^\bullet$. The precursor cation **1**$^+$ was generated by exothermic protonation of sulfur dioxide under conditions of chemical ionization in the gas phase. From the proton affinity of SO_2, PA = 635 ± 4 kJ mol^{-1} from the averaged experimental and G2(MP2)-calculated values, protonations with CH_5^+ (PA(CH_4) = 548 ± 3 kJ mol^{-1}) and H_3^+(PA(H_2) = 423 kJ mol^{-1}) were 87 and 212 kJ mol^{-1} exothermic, respectively. This implied that protonation with CH_5^+ formed exclusively the syn and anti rotamers of **1**$^+$, whereas the less stable isomers **2**$^+$−**4**$^+$ were energetically inaccessible. In contrast, protonation with H_3^+ could proceed exothermically to form both **1**$^+$ and **2**$^+$.

Collisional neutralization of **1**$^+$ was studied with dimethyl disulfide (DMDS, IE$_v$ = 8.96 eV), di-*n*-butylamine (DBA, IE$_v$ = 8.45 eV), and aniline (IE$_v$ = 8.03 eV) as electron donors.[50c] Hence, vertical electron transfer to **1**$^+$ from these molecules ranged from ∼0.5 eV endothermic to ∼0.5 eV exothermic. The NR mass spectra showed a prominent survivor ion of SO_2H^+ at *m/z* 65 for all three neutralization targets. The primary

(53) The UHF/6-31+G(d,p) frequency analysis of the transition state for the H−S bond cleavage in **2** yielded an impossibly high frequency for the H−S bending mode, as also reported by Binns and Marshall (ref 30). This was corrected by using a scaled wavenumber for the same vibration in **2**. The scaling factor of 0.75 was estimated from the wavenumbers of other bending modes in **2** and the transition state.

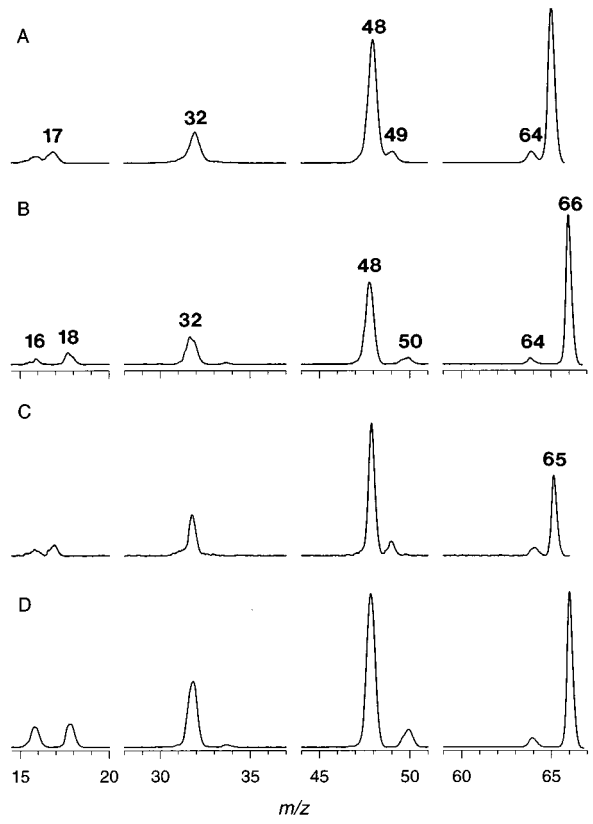

Figure 4. Neutralization−reionization (CH_3SSCH_3, 70% transmittance/O_2, 70% transmittance) mass spectra of (a) $\mathbf{1}^+$ by protonation with CH_5^+, (b) $\mathbf{1D}^+$ by deuteronation with CD_5^+. Neutralization−collisional activation−reionization (CH_3SSCH_3, 70%T/He, 70%T/O_2, 70%T) mass spectra of (c) $\mathbf{1}^+$, (d) $\mathbf{1D}^+$.

fragments in the spectra were $SO_2^{\bullet+}$ (*m/z* 64), SOH^+ (*m/z* 49), OH^+ (*m/z* 17), and $O^{\bullet+}$ (*m/z* 16). Loss of $OH^\bullet$ was the dominant dissociation upon NR, which amounted to 35−40% of the sum of NR ion intensities (%$\sum I_{NR}$) for all neutralizations (Figure 4a). The data showed that, for the 1 eV range of target ionization energies employed, there was no obvious correlation between the energetics of the electron transfer and the dissociation kinetics.[27]

Collisional activation with helium of the intermediate radicals **1** resulted in a diminished relative intensity of survivor $\mathbf{1}^+$, whereas the relative intensity ratios for the primary dissociation products did not change appreciably (Figure 4c). Increasing the probability of multiple collisions of **1** by decreasing the transmittance of the main beam from 70 to 50 and 30% resulted in a sequential decrease of the survivor ion relative intensity down to 23%$\sum I_{NR}$ at the lowest transmittance. Neutral collisional activation resulted in an increase of the relative abundances of S^+ and O^+, which were secondary dissociation products. However, the $[SO_2^{\bullet+}]/[SO^{\bullet+}]$ ratio showed no clear trend upon collisional activation under single or multiple collision conditions and remained essentially unchanged (∼0.1−0.13).

The NR spectra of $\mathbf{1D}^+$ (by deuteronation with CD_5^+/CD_4), obtained by neutralization with DMDS (Figure 4b), DBA, and aniline, showed increased relative abundances of survivor $\mathbf{1D}^+$ (46−50%$\sum I_{NR}$). The formation of $SO^{\bullet+}$ by loss of $OD^\bullet$ was the dominating dissociation, whereas loss of $D^\bullet$ was less abundant, giving $[SO_2^{\bullet+}]/[SO^{\bullet+}] = 0.06-0.1$. Collisional activation of neutral **1D** resulted in a diminished relative abundance of $\mathbf{1D}^+$ (34%), whereas the $[SO_2^{\bullet+}]/[SO^{\bullet+}]$ ratio did not change appreciably (0.06−0.07, Figure 4d).

Note that $SO_2^{\bullet+}$ was stable under CH_3SSCH_3/O_2 NR to give a survivor ion of 57%$\sum I_{NR}$. The low relative abundances of $SO_2^{\bullet+}$ in the NR spectra of $\mathbf{1}^+$ and $\mathbf{1D}^+$ were therefore due to inefficient losses of $H^\bullet$ or $D^\bullet$ and not to an instability or low reionization efficiency of SO_2 (see Experimental Section and below).

Dissociations of neutral **1** and reionized $\mathbf{1}^+$ were distinguished by variable-time NR mass spectra.[36] The time-dependent relative intensities of the reionized $\mathbf{1}^+$, $SO_2^{\bullet+}$, SOH^+, $SO^{\bullet+}$, and OH^+ were fitted into kinetic equations to yield unimolecular rate parameters for the neutral and ion dissociations.[36] Least-square fits were obtained for a single exponential decay in the neutral channel and a bimodal exponential decay including one fast ($k > 10^8$) and one slow ($k \sim 10^4-10^6$) dissociation. Correlation was sought for channels producing complementary fragments.[36c] Solving the equations required estimates of the ionization cross sections for SO_2, $SOH^\bullet$, SO, and $OH^\bullet$ relative to that of **1**. These were obtained from the atomic increment scheme of Fitch and Sauter,[54] as $\sigma(SO_2)/\sigma(\mathbf{1}) = 0.866$, $\sigma(SOH)/\sigma(\mathbf{1}) = 0.834$, $\sigma(SO)/\sigma(\mathbf{1}) = 0.784$, and $\sigma(OH)/\sigma(\mathbf{1}) = 0.256$. Absolute ionization cross sections were recently measured for electron-impact ionization of SO[55] and SO_2.[56] The ratio, $\sigma(SO)/\sigma(SO_2) = 0.97-0.87$ for 70−160 eV electrons, was reasonably close to that from the Fitch-Sauter scheme (0.91).

The formation of $SO^{\bullet+}$ and OH^+ showed predominant contributions from *neutral dissociations* followed by reionization, e.g., $k_N(OH^\bullet) = (3.1 \pm 0.6) \times 10^5\ s^{-1}$, $k_N(SO) = (3.5 \pm 0.4) \times 10^5\ s^{-1}$, from six measurements. The rate parameters correlated for both observation channels, which provided further unequivocal evidence for the neutral dissociation.[36c] The rate parameters for ion dissociations in reionized $\mathbf{1}^+$ were smaller, e.g., $k_i(OH^+) = (-0.2 \pm 0.4) \times 10^5\ s^{-1}$, $k_i(SO^{\bullet+}) = (1.6 \pm 0.6) \times 10^5\ s^{-1}$, and the values did not correlate because of the different ionization energies of the products.[36c] Best fits for k_N were obtained for the single exponential kinetic model, which indicated, although did not mandate, that most dissociations of **1** occurred on the microsecond time scale.

The rate parameters for the formation of neutral and ionic SO_2 were too small to give a definite answer as to the predominant nature of this dissociation, e.g., $k_N(SO_2) = (3.6 \pm 0.8) \times 10^4\ s^{-1}$ and $k_i(SO_2^{\bullet+}) = (2 \pm 2) \times 10^4\ s^{-1}$. Evidently, loss of $H^\bullet$ was disfavored in both **1** and reionized $\mathbf{1}^+$. Loss of O to give $SOH^\bullet$ also proceeded in neutral **1**, $k_N(SOH^\bullet) = (7 \pm 2) \times 10^4\ s^{-1}$, $k_i(SOH^+) = (0 \pm 4) \times 10^4\ s^{-1}$, although overall this dissociation was much slower than the loss of OH.

Different NR spectra were obtained for $[H,S,O_2]^+$ ions prepared by the more exothermic protonation with H_3^+ (Figure 5a). The spectra pointed to the presence of another isomer coformed with $\mathbf{1}^+$ by highly exothermic protonation, which was assigned structure $\mathbf{2}^+$, as discussed below. Collisional activation of a mixture of neutral **1** and **2** at 70 and 50% beam transmittance lowered the relative abundance of the survivor ion ($\mathbf{1}^+ + \mathbf{2}^+$), which decreased from 23%$\sum I_{NR}$ in the NR spectrum to 10%$\sum I_{NR}$ in the NCR spectrum at 50% precursor beam transmittance (Figure 5b). The relative intensities of low mass fragments increased substantially, e.g., $S^{\bullet+}$(15 to 26%$\sum I_{NR}$), $O^{\bullet+}$ (4 to 10%$\sum I_{NR}$), and OH^+ (0.5 to 3%$\sum I_{NR}$). The highly endothermic formations of these fragments must be due to multiple collisions whose probability, as calculated for a Poisson distribution,[57] increased from 17% at 70% beam transmittance to 31% at 50% beam transmittance. The branching ratio for

(54) Fitch, W. L.; Sauter, A. D. *Anal. Chem.* **1983**, *55*, 832−835.
(55) Tarnovsky, V.; Levin, A.; Deutsch, H.; Becker, K. *J. Chem. Phys.* **1995**, *102*, 770−773.
(56) Basner, R.; Schmidt, M.; Deutsch, H.; Tarnovsky, V.; Levin, A.; Becker, K. *J. Chem. Phys.* **1995**, *103*, 211−218.
(57) Holmes, J. L. *Org. Mass Spectrom.* **1985**, *20*, 169−183.

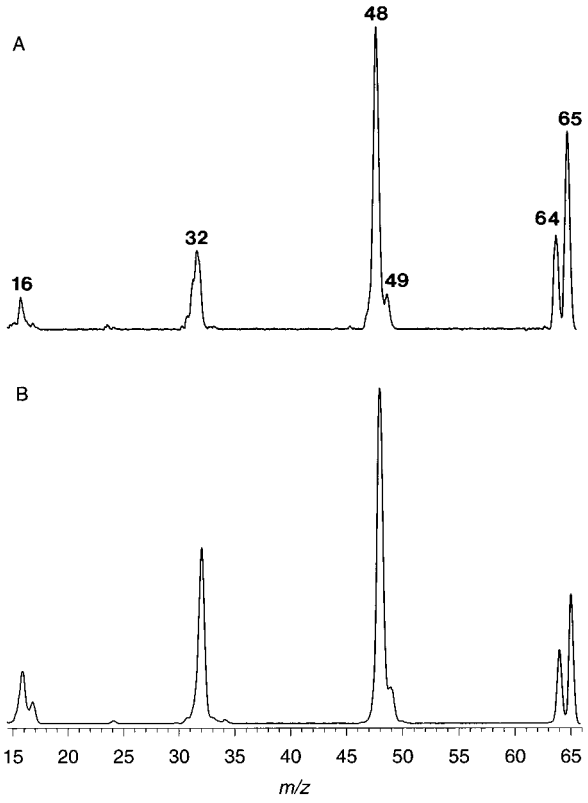

Figure 5. (a) Neutralization−reionization (CH_3SSCH_3, 70% transmitttance/O_2, 70% transmittance) mass spectrum of a mixture of $\mathbf{1}^+$ and $\mathbf{2}^+$ by protonation with H_3+. (b) Neutralization−collisional activation−reionization (CH_3SSCH_3, 70%T/He, 70%T/O_2, 70%T) mass spectrum of $\mathbf{1}^+$ and $\mathbf{2}^+$.

$[SO_2^{\bullet+}]/[SO^{\bullet+}]$ decreased from 0.26 in the NR spectrum to 0.16−0.17 following neutral collisional activation.

The nature of these dissociations was further examined by variable-time measurements, which gave the following results. Loss of $H^\bullet$ proceeded mainly in *neutral* $[H,S,O_2]^\bullet$, $k_N(SO_2) = 1.5 \times 10^5\ s^{-1}$, $k_i(SO_2^{\bullet+}) = 0.4 \times 10^5\ s^{-1}$. The H^+ channel could not be followed because of the quadrupole analyzer low-mass cutoff. Loss of O was also a predominantly neutral dissociation, $k_N(SOH^\bullet) = 1.6 \times 10^5\ s^{-1}$. The loss of OH showed correlating rate parameters for both neutral products, e.g., $k_N(SO) = 6.3 \times 10^5\ s^{-1}$ and $k_N(OH) = 5.4 \times 10^5\ s^{-1}$. The rate parameter for the ion dissociation was obtained for the $SO^{\bullet+}$ channel only, $k_i(SO^{\bullet+}) = 1 \times 10^5\ s^{-1}$. Hence, post-reionization dissociation represented a minor channel for the $SO^{\bullet+}$ formation.

Laser Photoexcitation of $SO_2H^\bullet$. Irradiation of the neutralized beam of **1** with the 488 and 514.5 nm lines was performed for total laser outputs of 5.5, 8.1, and 11.1 W. Exposure of the neutral beam to 2.41 and 2.54 eV photons resulted in ±20% changes in the total NR ion current and visible changes in the ion relative intensities. To compensate for the variations in the total NR ion currents, the ion intensities were scaled to the same total ion count, and the scaled spectra obtained with laser on and laser off were subtracted. The differential intensities for the individual species were normalized to the NR ion intensity in the laser-off spectrum and the averaged results were summarized in Figure 6a,b.

Since both the neutral beam and the ions formed by reionization were exposed to the laser beam, the possibility of ion photofragmentation must be considered. At 488−514.5 nm, $SO_2^{\bullet+}$ and $SO^{\bullet+}$ were transparent as judged from the energy levels in the photoelectron spectra.[58,59] The closed-shell ion $\mathbf{1}^+$ was presumed to be transparent above 350 nm by analogy

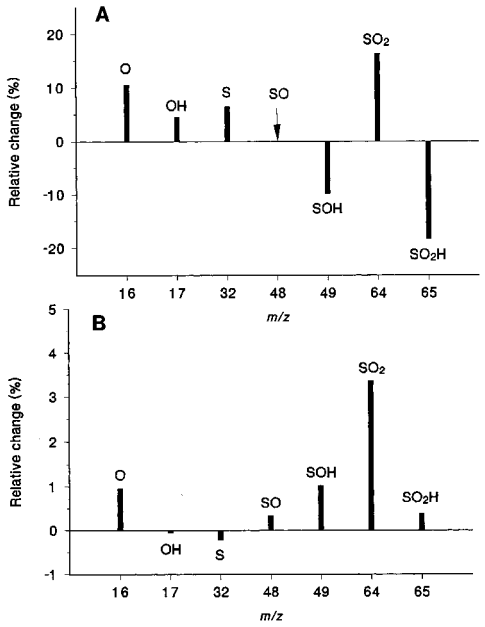

Figure 6. Normalized difference spectra for photodissociation of (a) **1**, (b) **1** and **2**.

with SO_2.[60] For SOH^+, two low-lying excited states ($^1A'$ and $^1A''$) were 0.6−0.7 eV above the $^3A''$ ground electronic state, whereas the excited-state manifold in the 2.4−2.5 eV region above the $^3A''$ state was unknown.[14] Thus, depletion by ion photofragmentation of the SOH^+ intensity upon irradiation could not be excluded.

The difference spectrum for **1** showed diminished relative intensities of $\mathbf{1}^+$ and SOH^+ and increased relative intensities of $SO_2^{\bullet+}$, $S^{\bullet+}$, OH^+, and $O^{\bullet+}$, whereas the abundant $SO^{\bullet+}$ ion was practically unchanged (Figure 6a). In the absence of ion photofragmentations, the photoexcitation experiments clearly showed that a fraction of **1** formed by collisional neutralization absorbed in the 2.41−2.54 eV energy range. Photofragmentation of **1** resulted in an enhancement of loss of $H^\bullet$ whereas the loss of $OH^\bullet$ was not affected. The time-dependence of neutral photofragmentations was investigated for the 0.3−2.8 μs and 3.8 μs observation times. The difference spectra for the longer observation time showed greater changes in the product relative intensities, especially in the depletion of **1** and increased formation of SO_2. However, the directions of these changes were the same in both series of measurements.

The difference spectrum for the mixture of **1** and **2** showed in general smaller changes upon irradiation (Figure 6b). The latter spectrum showed a small increase in the $[H,S,O_2]^+$ and SOH^+ peaks upon photoexcitation. The major net change, due to irradiation, was the relative increase in the intensity of $SO_2^{\bullet+}$.

Discussion of $[H,S,O_2]^\bullet$ Dissociations. We address the apparently contradicting data from the ab initio/RRKM calculations and mass spectrometric experiments. The vibrational energy of $(^2A'')\mathbf{1}$ formed by vertical neutralization of $\mathbf{1}^+$ could be bracketed between 31 and 96 kJ mol^{-1} from combining the range of internal energies available to $\mathbf{1}^+$ and the Franck−

(58) Kimura, K.; Katsumata, S.; Achiba, Y.; Yamazaki, T.; Iwata, S. *Handbook of He(I) Photoelectron Spectra of Fundamental Organic Molecules*; Japan Scientific Societies Press: Tokyo, 1981; pp 40−41.

(59) (a) Dyke, J. M.; Golob, L.; Jonathan, N.; Morris, A.; Okuda, M.; Smith, D. J. *J. Chem. Soc., Faraday Trans. II* **1974**, *70*, 1818−1827 (b) Golob, L.; Jonathan, N.; Morris, A.; Okuda, M.; Ross, K. J.; Smith, D. J. *Ber. Bunsenges. Phys. Chem.* **1974**, *78*, 201.

(60) Estimated from the absorption maximum of sulfur dioxide, $\lambda_{max} = 300$ nm. See: (a) Millan, M. M.; Hoff, R. M. *Appl. Opt.* **1977**, *16*, 1609−1618. (b) *Handbook of Air Pollution Analysis*; Harrison, R. M., Perry, R., Eds.; Chapman & Hall: London, 1986; p 466.

Condon energy due to the electron transfer.[61] This vibrational energy alone was insufficient to promote dissociations of **1** following neutralization. Even under an assumption that more vibrational energy could have been deposited into **1** via some other collisional mechanism, the RRKM rate constants would predict predominant dissociation by loss of H$^\bullet$ up to ~325 kJ mol^{-1} excitation. This clearly contradicted the experimental data, which showed the loss of OH$^\bullet$ to be the dominating neutral dissociation. To account for the substantial fraction of nondissociating radicals (>35%) and the fraction dissociating by loss of OH$^\bullet$, one would have to consider a sharply bimodal internal energy distribution in **1** with a gap in the 210−314 kJ mol^{-1} energy range. Barring this unlikely scenario, the observed and resolved neutral dissociations were incompatible with the properties of the potential energy surface for the ^{2}A″ ground electronic state. This led to the inevitable conclusion that *most of the observed neutral dissociations in* ***1*** *proceeded from excited electronic states*. Excited states were accessible owing to the nonresonant character of collisional electron transfer and the absence of spin or dipole selection rules. Although excited electronic states in radicals have been recognized to participate in NR dissociations,[23,37,64] the present finding of their dominant role was unprecedented.

The exact manifold of excited states in **1** could not be examined by ab initio calculations because of the difficulties mentioned above. However, the experimental data provided some qualitative characterization. The single-exponential decay in the main dissociation channel to SO and OH$^\bullet$, which showed microsecond kinetics, implied that this dissociation must have had a substantial activation barrier. Hence, the relevant excited electronic state(s) of **1** must be bound. Further insight was provided by the dissociations observed for neutral collisional activation and photoexcitation, which both involved electronic excitation. Collisional activation of small ions or molecules at keV kinetic energies is thought to result in non-selective electronic excitation, due to the short time for energy transfer during the collision (<10^{-14} s).[65] Single-photon absorption is inherently a state-to-state process. The two methods thus provided complementary approaches to studying electronic excitation in transient neutral intermediates. The NCR and photoexcitation spectra of **1** showed different changes in product formations. The state-selective photoexcitation promoted formation of SO_2, whereas the energy-nonselective collisional excitation preserved the [SO_2]/[SO] branching ratio. Photoexcitation from the ^{2}A″ ground state of **1** could not proceed to the ^{2}A′ excited state because of the 4.3 eV energy gap. However, the photon energies would be sufficient to promote isomerization to **2**, which would be followed by rapid dissociation to SO_2 and H$^\bullet$. For this to occur, the first ^{2}A″ excited state must be only 2.4−2.54 eV above the X(^{2}A″) state to allow laser light absorption. However, it was difficult to explain why such an excited state was not accessed by the nonselective collisional excitation. Hence, the interpretation invoking a low lying ^{2}A″ excited state did not satisfy both sets of experimental data.

A more plausible interpretation stemmed from the different selectivities of photoexcitation and collisional activation. The latter process is nonselective, includes both the (X)^{2}A″ ground state (>35%) and the metastable excited states of **1**, and can populate dissociative electronic states similar to those produced upon neutralization. By contrast, photoexcitation was selective in that only metastable excited states of **1** could absorb energy at the wavelengths used. The specific enhancement of the H-loss channel was likely to be due to the reactivities of higher excited states of **1**. It would be desirable to conduct photoexcitations with a tunable laser to obtain the energies of all accessible excited states in **1**. Unfortunately, the number of radicals in the photoexcitation volume of the neutralized beam was on the order of 10^4, corresponding to a 10^{-14} Torr equivalent partial pressure. High photon fluxes and duty cycles are therefore necessary to achieve photoexcitation, which are currently unavailable from tunable lasers.

The highly exothermic protonation of sulfur dioxide with H_3^+ could form both $\mathbf{1}^+$ and the less stable isomer $\mathbf{2}^+$; the NR spectrum of thus formed ions indicated the presence of another [H,S,O_2]$^\bullet$ isomer. The calculated energies showed that **2** formed by collisional neutralization should lose H$^\bullet$ as the predominant dissociation. The enhancement of this dissociation channel in the NR spectrum was therefore consistent with the presence of **2**. In contrast, $\mathbf{1}^+$ from H_3^+-protonation should have left the ion source with 130 kJ mol^{-1} of average vibrational energy.[61] However, even if supplied with 26 kJ mol^{-1} of Franck−Condon energy upon neutralization (vide supra), this combined internal energy of **1** would be insufficient to drive isomerization to **2** and lead to loss of H$^\bullet$. The combined experimental and energy data thus indicate coformation of **2**. The variable-time measurements further identified neutral dissociation of [H,S,O_2] to SO, which pointed to the presence of excited **1**. Hence both **1** and **2** were formed in a mixture.

Ion and Neutral Energetics in the [H_2,S,O_2] System. Cation-radicals and molecules of the [H_2,S,O_2] group were addressed by ab initio calculations to characterize the isomers produced by dissociative ionization in the gas phase and to obtain relative energies for unimolecular dissociations and isomerizations. The MP2(FULL)/6-31+G(d,p) optimized structures are shown in Figures 7 and 8, the relative enthalpies for the cation-radicals are summarized in Table 3.

The cation-radical of dihydroxysulfane ($\mathbf{6}^{\bullet+}$) was found to exist as two stable rotamers of C_{2v} ($\mathbf{6a}^{\bullet+}$) and C_1 ($\mathbf{6b}^{\bullet+}$) symmetry (Figure 7). The C_{2v} structure $\mathbf{6a}^{\bullet+}$ was only marginally more stable than $\mathbf{6b}^{\bullet+}$ by 0.3 kJ mol^{-1} at 0 K. This order of stabilities resulted from inclusion in the G2(MP2) scheme of the MP2/6-311+G(3df,2p) calculation, whereas the other calculations that used smaller basis sets slightly favored the C_1 structure. The rotamers were separated by a small rotational barrier, which was calculated with UMP2/6-31+G(d,p) as 6.5 kJ mol^{-1} above $\mathbf{6b}^{\bullet+}$. Rotation about the S−O bond was thus very facile, and the rotamers were predicted to coexist as a 55/45 mixture at 298 K. A third C_{2v} or C_2 rotamer with a syn−syn orientation of the O−H bonds was also sought computationally but was not found as a local energy minimum.

Other [H_2,S,O_2]$^{\bullet+}$ valence-bond isomers were found to be substantially less stable than $\mathbf{6}^{\bullet+}$ (Table 3). The sulfone structure $\mathbf{8}^{\bullet+}$ (C_s) showed substantially different S−O bond lengths (Figure 7), which indicated a single-bond character for the long S−O bond and a double-bond character for the short one. Mullikan population analysis of $\mathbf{8}^{\bullet+}$ (^{2}A″) showed that the distant

(61) The upper limit for the vibrational energies in $\mathbf{1}^+$ and $\mathbf{2}^+$ were estimated from 80% of protonation exothermicity deposited in the ion (ref 62). The lower limit was estimated from the product heat capacities, e.g., 62% and 57% of the protonation exothermicity for protonations with H_3^+ and CH_5^+, respectively. Collisional de-excitation was estimated for an average of 70 collisions in the ion source (ref 63).

(62) Uggerud, E. *Adv. Mass Spectrom.* **1995**, *13*, 53−70.

(63) (a) Abel, B.; Herzog, B.; Hippler, H.; Troe, J. *J. Chem. Phys.* **1989**, *91*, 900−905. (b) Gilbert, R. G.; Smith, S. C. *Theory of Unimolecular and Recombination Reactions*; Blackwell: Oxford, 1990; p 254.

(64) Shaffer, S. A.; Turecek, F. *J. Am. Chem. Soc.* **1994**, *116*, 8647−8653.

(65) (a) *Collision Spectroscopy*; Cooks, R. G., Ed.; Plenum Press: New York, 1979. (b) Todd, P. J.; McLafferty, F. W. In *Tandem Mass Spectrometry*; McLafferty, F. W., Ed.; Wiley: New York, 1983.

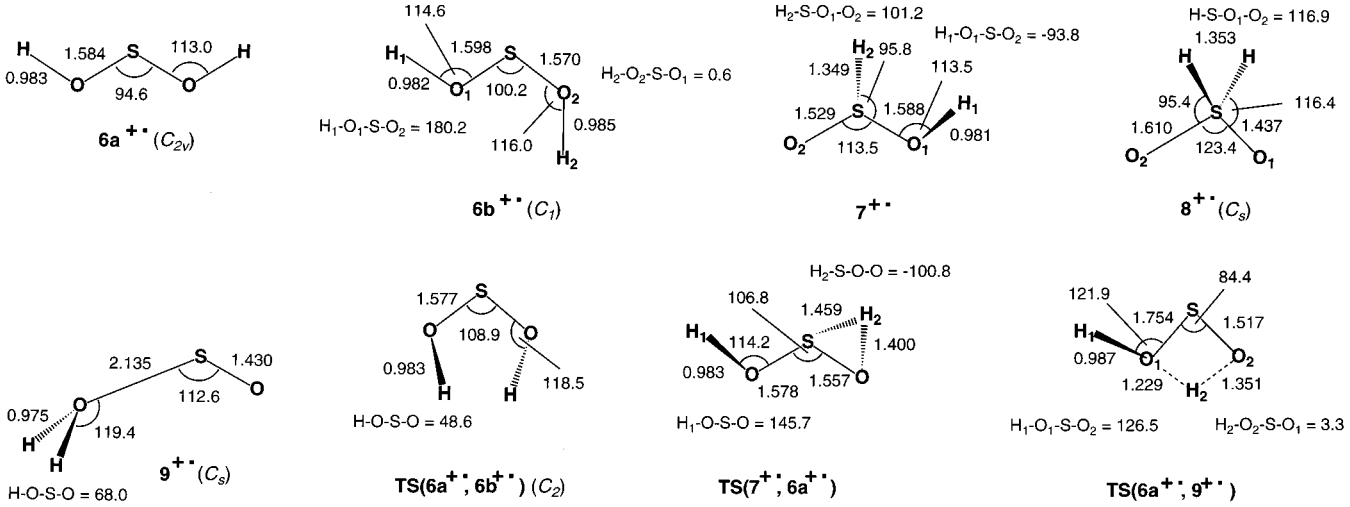

Figure 7. UMP2(FULL)/6-31+G(d,p) optimized structures of $[H_2,S,O_2]^{\bullet+}$ cation-radicals.

Table 3. Relative Enthalpies of $[H_2,S,O_2]^{\bullet+}$ Ions[a]

ion/reaction	ΔH_0	ΔH_{298}
6a$^{\bullet+}$	0	0
6b$^{\bullet+}$	0.2	0.3
6b$^{\bullet+}$ (VI)[b]	57	
7$^{\bullet+}$	150	148
8$^{\bullet+}$	352	349
9$^{\bullet+}$	19	20
TS(**6a**$^{\bullet+}$ → **6b**$^{\bullet+}$)	6[c]	6[c]
TS(**6a**$^{\bullet+}$ → **7**$^{\bullet+}$)	237	235
TS(**6a**$^{\bullet+}$ → **9**$^{\bullet+}$)	147	144
TS(**7**$^{\bullet+}$ → **9**$^{\bullet+}$)	264	262
6a$^{\bullet+}$ → *syn*-**1**$^{+}$ + H$^{\bullet}$	234	238
6a$^{\bullet+}$ → SO$^{\bullet+}$ + H_2O	166	171
6a$^{\bullet+}$ → (^{3}A″)SOH$^+$ + OH$^{\bullet}$	357	363

[a] From G2(MP2) energies in kJ mol^{-1}. [b] Vertical ionization of **6b**. [c] From MP2(FULL)/6-31+G(d,p) calculations.

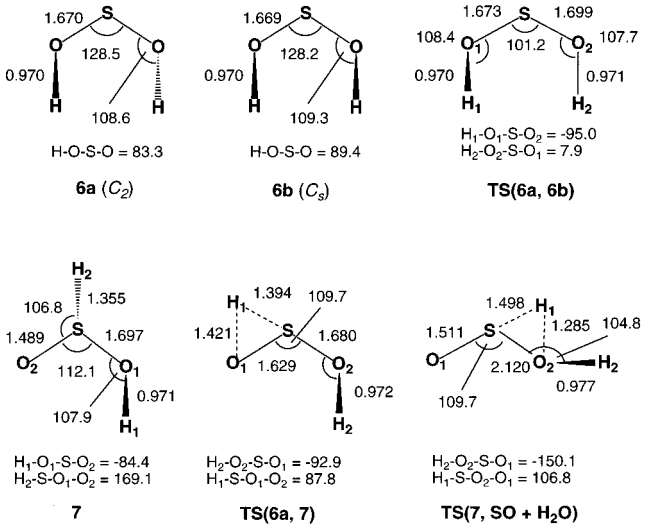

Figure 8. MP2(FULL)/6-31+G(d,p) optimized structures of $[H_2,S,O_2]$.

oxygen atom (O-2) carried 98% of the spin density, whereas the sulfur atom carried a large positive atomic charge (+1.28). Thus, cation-radical **8**$^{\bullet+}$ could be viewed as a distonic ion,[66] in which the unpaired electron density and the positive charge were localized at different atoms. Ion **7**$^{\bullet+}$ showed a similar distonic character with 97% spin density localized on the oxygen terminus (O-2) and +1.36 atomic charge localized on sulfur. A similar separation of spin and positive charge densities was found previously for oxygenated phosphorus cation-radicals and used to explain the high reactivity in hydrogen atom abstraction reactions.[67]

In addition to the classic valence-bond isomers **6**$^{\bullet+}$−**8**$^{\bullet+}$, the computations also localized structure (**9**$^{\bullet+}$), which was characterized by a long S−O bond and could be described as an ion−molecule complex between SO$^{\bullet+}$ and water (Figure 7). Ion **9**$^{\bullet+}$ was only 19 kJ mol^{-1} less stable than **6a**$^{\bullet+}$ at 0 K and was bound by 147 kJ mol^{-1} against dissociation to SO$^{\bullet+}$ and H_2O (Table 3).

Transition states were located for the unimolecular isomerizations of **6a**$^{\bullet+}$ to **7**$^{\bullet+}$, **7**$^{\bullet+}$ to **9**$^{\bullet+}$, and **6a**$^{\bullet+}$ to **9**$^{\bullet+}$ (Figure 7). The energies are summarized in Table 3. It is noteworthy that the energy barrier for the **6a**$^{\bullet+}$ → **9**$^{\bullet+}$ isomerization was below the calculated thermochemical threshold for dissociation to SO$^{\bullet+}$ and H_2O (166 kJ mol^{-1}, Table 3). Hence, a small fraction of **6a**$^{\bullet+}$ with internal energies in the 147−166 kJ mol^{-1} range could isomerize reversibly to **9**$^{\bullet+}$ (vide infra).

Bond cleavage dissociations in **6a**$^{\bullet+}$ were found to be substantially endothermic (Table 3). Cleavage of the S−O bond to give (^{3}A″)SOH$^+$ and OH$^{\bullet}$ required 357 kJ mol^{-1}, whereas cleavage of the O−H bond to give *anti*-**1**$^+$ and H$^{\bullet}$ required 235 kJ mol^{-1} at 0 K. Hence, elimination of water was the lowest-energy unimolecular dissociation of **6a**$^{\bullet+}$ (Table 3). Stable ions **6**$^{\bullet+}$ sampled for collisional neutralization must therefore have internal energies <147 kJ mol^{-1}.

Two stable rotamers were found for neutral dihydroxysulfane **6**, e.g., the C_2 structure **6a** and the C_s structure **6b** (Figure 8). Of these, the latter was less stable by 5 kJ mol^{-1} at 0 K. Rotamers **6a** and **6b** were separated by a barrier to rotation about the S−O bond, which was calculated at 39 kJ mol^{-1} by MP2-(FULL)/6-31+G(d,p). The calculated ΔG°_{298}(**6a** → **6b**) = 3.3 kJ mol^{-1} indicated a 79/21 mixture of rotamers **6a** and **6b** at thermal equilibrium. An attempted UHF/6-31+G(d,p) optimization of a triplet state of **6** resulted in S−O bond cleavage and dissociation to OH$^{\bullet}$ and SOH$^{\bullet}$. Hence the existence of a stable triplet **6** was not supported at this level of theory.

Other $[H_2,S,O_2]$ isomers were studied previously and found to be substantially less stable than **6a,b**.[34,35] We examined the second most stable isomer **7**, which was calculated to be 20 kJ mol^{-1} less stable than **6a** at 0 K (Table 4). However, **7** was separated from **6a** by a large isomerization barrier (Table 4). A

(66) Radom, L.; Bouma, W. J.; Nobes, R. H.; Yates, B. F. *Pure Appl. Chem.* **1984**, *56*, 1831−1842. For reviews see: (a) Hammerum, S. *Mass Spectrom. Rev.* **1988**, *7*, 123−202. (b) Stirk, K. M.; Kiminkinen, L. K. M.; Kenttamaa, H. I. *Chem. Rev.* **1992**, *92*, 1649−1666.

(67) Turecek, F.; Gu, M.; Hop, C. E. C. A. *J. Phys. Chem.* **1995**, *99*, 2278−2291.

similar barrier was obtained for the hydrogen transfer and elimination of water from **7**. Dissociations by simple bond cleavage in **6a** were all substantially endothermic. Cleavage of the O−H bond required 253 kJ mol^{-1} to give *syn*-**1** and H$^{\bullet}$, whereas cleavage of the S−O bond required 311 kJ mol^{-1} (Table 4). The lowest threshold energy was found for the spin-forbidden formation of ($^3\Sigma^-$)SO and H_2O (43 kJ mol^{-1}), whereas the spin-allowed formation of ($^1\Delta$)SO and H_2O required 125 kJ mol^{-1} at the thermochemical threshold at 0 K. Attempts to find the transition state for the direct elimination of water from **6a** were unsuccessful, and so the question of whether this reaction pathway can compete with the stepwise elimination of water remains open.

The thermochemical thresholds for the dissociations of O−H and S−O bonds in **6a** were calculated at 253 and 311 kJ mol^{-1}, respectively, above **6a**. Thus both dissociations were predicted to be substantially endothermic. The potential energy along the O−H coordinate was investigated by MP2(FULL)/6-31+G-(d,p) calculations, which showed an energy barrier of ∼100 kJ mol^{-1} above the products at a relatively large O−H separation of 2.215 Å.

Ionization and neutralization in the [H_2,S,O_2] system were of relevance to the NR experiments and were therefore addressed computationally. The adiabatic ionization energies of **6a** and **6b** were very similar, 8.90 and 8.86 eV, respectively. Vertical ionization of **6a** showed IE_v = 9.50 eV, implying a deposition of 57 kJ mol^{-1} vibrational energy in the ion through Franck−Condon effects. The vertical recombination energy of **6a**$^{\bullet+}$, RE_v = 7.95 eV, indicated that vertically formed **6a** should on average attain 92 kJ mol^{-1} of internal energy to be converted to vibrational excitation. This corresponded to an effective temperature of 1270 K at which point the rotamers **6a** and **6b** were completely equilibrated at a 55/45 ratio. The IE_a(**7**) was calculated at 10.25 eV. This relatively high value was due mainly to the substantial destabilization of **7**$^{\bullet+}$ against **6**$^{\bullet+}$ (vide supra).

Compared with the previous MP4/6-31G(d) calculations of Laakso and Marshall,[35] the present G2(MP2) data showed substantially different relative energies. In particular, the energy difference between **6a** and **7** and the transition state energy for the **6a** → **7** isomerization were 35−36 kJ mol^{-1} smaller at the G2(MP2) level, whereas the dissociation to *syn*-**1** and H$^{\bullet}$ was 72 kJ mol^{-1} more endothermic by the present calculations. The relative energy of **6a** at 298 K was anchored to the standard heats of formation of ($^3\Sigma^-$)SO and H_2O (eq 2) and isodesmic reactions (eqs 3 and 4) to provide $\Delta H_{f,298}$(**6a**) = −277 ± 3 kJ mol^{-1}.

$$\mathbf{6a} \rightarrow (^3\Sigma^-)\mathrm{SO} + \mathrm{H_2O} \quad \Delta H_{r,298} = 43 \text{ kJ mol}^{-1} \qquad (2)$$

$$\mathbf{6a} + (^3\Sigma^-_g)\mathrm{O_2} \rightarrow \mathrm{SO_2H^{\bullet}} + {}^{\bullet}\mathrm{OOH} \quad \Delta H_{r,298} = 43 \text{ kJ mol}^{-1} \qquad (3)$$

$$\mathbf{6a} + \mathrm{OH^{\bullet}} \rightarrow \mathrm{SO_2H^{\bullet}} + \mathrm{H_2O} \quad \Delta H_{r,298} = -247 \text{ kJ mol}^{-1} \qquad (4)$$

The Boltzmann-averaged heat of formation for dihydroxysulfane, **6**, was obtained from the 298 K populations of **6a** and **6b** (ΔG_{298}(**6a** → **6b**) = 3.3 kJ mol^{-1}) as −276 ± 3 kJ mol^{-1}.

RRKM Kinetics in the [H_2,S,O_2] System. The close energies of **6a,b**$^{\bullet+}$ and **9**$^{\bullet+}$ and the fact that the energy barrier to their interconversion was below the dissociation threshold for elimination of water raised the question of isomer equilibration. In particular, ions with internal energies between the isomerization barrier and the dissociation threshold could isomerize to achieve equilibrium populations. The equilibrium constant, $K_{eq} = k_1/k_{-1}$, was calculated from the RRKM rate constants for the forward (k_1) and reverse k_{-1} isomerization, where the forward reaction referred to **6b**$^{\bullet+}$ → **9**$^{\bullet+}$. The K_{eq} for the fraction of interconverting ions showed a very flat dependence on the ion internal energy, e.g., 0.078−0.073, for the 18.5 kJ mol^{-1} energy range between the isomerization barrier and the dissociation threshold. This implied that <7% of nondissociating **6a,b**$^{\bullet+}$ with sufficient internal energies could isomerize to **9**$^{\bullet+}$. The stepwise isomerization, **6a,b**$^{\bullet+}$ → **7**$^{\bullet+}$ → **9**$^{\bullet+}$, had large energy barriers in both steps and could not compete with the **6a,b**$^{\bullet+}$ ⇄ **9**$^{\bullet+}$ reaction. Considering the substantial fraction of nonisomerizing **6a,b**$^{\bullet+}$ with internal energies below the isomerization barrier to **9**$^{\bullet+}$ (147 kJ mol^{-1}), it was safe to conclude that nondissociating **6**$^{\bullet+}$ existed predominantly (>95%) as rotamers **6a**$^{\bullet+}$ and **6b**$^{\bullet+}$, whereas reversible equilibration with other structures was negligible.

The very similar energy barriers for the isomerizations of **6** → **7** and for the further dissociation, **7** → ($^1\Delta$)SO + H_2O, also raised the question of the kinetics for the overall reaction, **6** ⇄ **7** → ($^1\Delta$)SO + H_2O. RRKM rate constants for **6** → **7** (k_1), **7** → **6** (k_{-1}), and **7** → SO + H_2O (k_2) were calculated for a range of internal energies and used to evaluate the time dependent populations of **6**, **7**, and the products. The calculations showed that the **6** → **7** isomerization was the rate determining step, which was slower than both the reverse reaction (k_1/k_{-1} = 0.31−0.58) and the dissociation to SO and H_2O (k_2/k_1 = 0.40−0.57). Reverse isomerization in dissociating **6** was therefore possible, although the calculated [**7**]/[**6**] ratio remained relatively low (0.18−0.25) because of the irreversible dissociation to the products.

Formation and Dissociations of SO_2H_2. Precursor ions **6**$^{\bullet+}$ were generated by dissociative ionization of dimethyl sulfate at 70 eV (Scheme 2)[23] and characterized by exact mass measurements (measured 65.9778, calc. 65.9776) and a CAD spectrum, which showed SO$^{\bullet+}$ and SOH$^+$ as the main fragment ions in a 2:1 ratio. The dissociation was facilitated by the high hydrogen atom affinities of the oxygen atoms in the cation-radical of dimethyl sulfate and in the intermediate formed by the elimination of formaldehyde that directed the hydrogen transfer to eventually form **6**$^{\bullet+}$. Formation of the most stable isomer **6**$^{\bullet+}$ was thus likely based on both the reaction thermochemistry and mechanism. Deuterium labeled ion **6D**$^{\bullet+}$ was prepared analogously from di(methyl-d_3) sulfate (Scheme 2).

Collisional neutralization of **6**$^{\bullet+}$ resulted in the formation of stable **6**, which showed a survivor ion following reionization (Figure 9). The NR mass spectra obtained by neutralizations with DBA, aniline, and DMDS were similar and showed survivor ion relative abundances in the 19−22%$\sum I_{NR}$ range. The primary dissociations were elimination of water, loss of OH$^{\bullet}$, and loss of H$^{\bullet}$. The effects of the dissociation energetics

Table 4. Relative Enthalpies of [H_2,S,O_2] Neutrals[a]

species/reaction	ΔH_0	ΔH_{298}
6a	0	0
6a(VN)[b]	93	
6b	5	5
6b(VN)[b]	87	
7	20	20
6a → *syn*-**1** + H$^{\bullet}$	253	259
6a → SOH$^{\bullet}$ + OH$^{\bullet}$	311	319
6a → ($^3\Sigma^-$)SO + H_2O	43	50
6a → ($^1\Delta$)SO + H_2O	125	133
TS(**6a** → **6b**)	39[c]	39[c]
TS(**6a** → **7**)	215	216
TS(**7** → ($^1\Delta$)SO + H_2O)	216	216

[a] From G2(MP2) energies in kJ mol^{-1}. [b] Vertical neutralization. [c] From MP2(FULL)/6-31+G(d,p) calculations.

Scheme 2

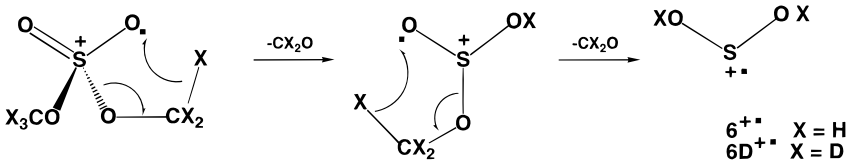

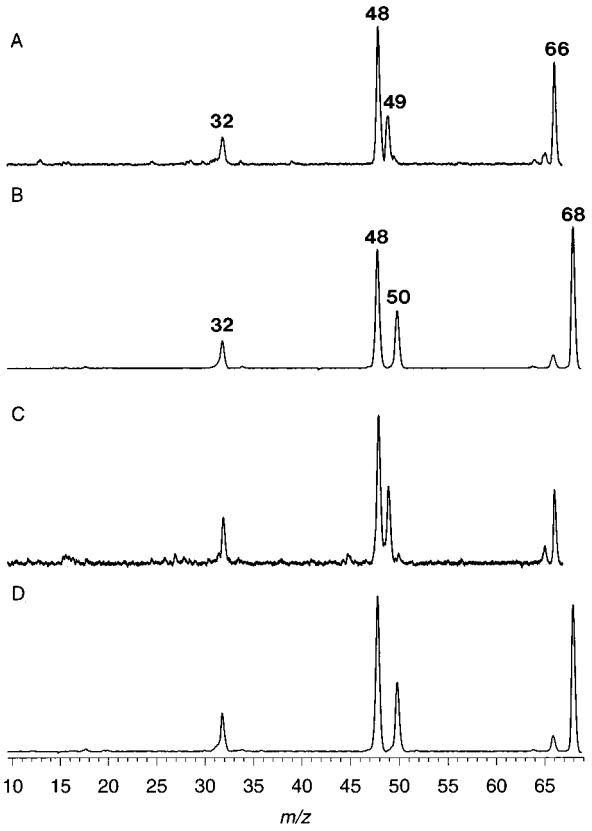

Figure 9. Neutralization−reionization (CH_3SSCH_3, 70% transmittance/O_2, 70% transmittance) mass spectra of (a) $\mathbf{6}^{\bullet+}$, (b) $\mathbf{6D}^{\bullet+}$. Neutralization−collisional activation (He, 70% transmittance)−reionization mass spectra of (c) $\mathbf{6}^{\bullet+}$, (d) $\mathbf{6D}^{\bullet+}$.

on the formation of $\mathbf{6}^{\bullet+}$ were examined by conducting the ionization with 20-eV electrons or by charge exchange with $N_2^{\bullet+}$ (IE = 15.58 eV). The NR mass spectra of thus prepared $\mathbf{6}^{\bullet+}$ showed slightly lower survivor ions (13−16%$\sum I_{NR}$) and somewhat higher $[SOH^+]/[SO^{\bullet+}]$ ratio (0.45) than did the spectra in Figure 9a (0.39). Deuterium in $\mathbf{6D}^{\bullet+}$ led to stabilization such that the NR spectra of $\mathbf{6D}^{\bullet+}$ showed survivor ions of 39−45%$\sum I_{NR}$ depending on the neutralization target. Neutralization with DMDS, which was 1 eV endothermic, gave the highest proportion of survivor ions for both $\mathbf{6}^{\bullet+}$ and $\mathbf{6D}^{\bullet+}$ (Figure 9a,b). The branching ratio for $[SOD^+]/[SO^{\bullet+}] = 0.44$ from $\mathbf{6D}^{\bullet+}$ was only slightly higher than from $\mathbf{6}^{\bullet+}$ under the same NR conditions (0.39), which indicated a small isotope effect on the elimination of water. Collisional activation at 70% transmittance of neutral **6** and **6D** was not very efficient (Figure 9c,d) and resulted in a slight increase of $[SOH,D^+]/[SO^{\bullet+}]$ to 0.52 and 0.48, respectively.

Variable-time measurements gave the following results. Dissociation of neutral **6** to $SOH^{\bullet}$ and $OH^{\bullet}$ was observed in both channels with correlating rate parameters, $k_N(SOH) = (2.3 \pm 0.5) \times 10^5\ s^{-1}$, $k_N(OH) = (3 \pm 2) \times 10^5\ s^{-1}$. The ion dissociation, $\mathbf{6}^{\bullet} \rightarrow SOH^+ + OH^{\bullet}$, was observed for $k_i(SOH^+) = (1.4 \pm 1.3) \times 10^5$. Hence, cleavage of the S−OH bond occurs in both neutral **6** and reionized $\mathbf{6}^{\bullet+}$. SO was formed by neutral dissociations, $k_N(SO) = (4.3 \pm 0.4) \times 10^5\ s^{-1}$, while the rate parameter for the complementary H_2O was very small, $k_N(H_2O) = 4 \times 10^4\ s^{-1}$. This indicated that the formation of SO could be due to consecutive dissociation $\mathbf{6} \rightarrow SOH \rightarrow SO$; the latter dissociation is known to occur upon NR.[17] Loss of water from reionized $\mathbf{6}^{\bullet+}$ gave $k_i(SO^{\bullet+}) = (3 \pm 2) \times 10^5\ s^{-1}$. Note that elimination of water is the dominating dissociation of $\mathbf{6}^{\bullet+}$ upon CAD. Losses of $H^{\bullet}$ and H_2 gave small rate parameters for both neutral and ion dissociations, which were consistent with the low relative abundance of SO_2H^+ and $SO_2^{\bullet+}$ in the spectra. In summary, the variable-time measurements found loss of OH occurring in dissociations of both neutral **6** and reioinized $\mathbf{6}^{\bullet+}$. Elimination of water is predominantly an ion dissociation occurring after reionization.

Conclusions

This combined computational and experimental study led to the important conclusion that a major fraction of hydroxysulfinyl radicals was formed in excited electronic states upon collisional electron transfer. The potential energy surface of the $(X)^2A''$ ground state was characterized in detail by ab initio/RRKM calculations and failed to explain the kinetics of neutral dissociations observed in the NR spectra. Nonselective collisional excitation and state-selective photoexcitation of stable radicals in their various electronic states were shown to result in different branching ratios for unimolecular dissociations. This provided experimental evidence that metastable excited states play an important role in the formation of transient species by fast collisional electron transfer.

Acknowledgment. Generous support of this work by a grant from the National Science Foundation (CHE-9412774) is gratefully acknowledged. Additional support by the Yu-Kong Corporation is also acknowledged. A.J.F. thanks Chevron Research for a fellowship during which tenure this work was performed. The computations were conducted using the resources of the Cornell Theory Center, which used to receive major funding from the National Science Foundation and New York State with additional support from the Advanced Research projects Agency, the National Center for Research Resources at the National Institutes of Health, IBM Corporation, and members of the Corporate Research Institute.

Supporting Information Available: Tables of uncorrected harmonic vibrational frequencies and ab initio, zero-point vibrational, and thermal energies for the molecules and ions under study (9 pages). See any current masthead page for ordering and Internet access instructions.

JA972602X